International Journal of GEOMATE, Dec., 2017, Vol. 13, Issue 40, pp. 173-182
Special Issue on Science, Engineering & Environment, ISSN: 2186-2990, Japan
DOI: https://doi.org/10.21660/2017.40.79849

UNMANNED ROTORCRAFT IN AGGRESSIVE ENVIRONMENT: AERODYNAMIC FLOW PERFORMANCE AGAINST WIND GUST

Ziad Bin Abdul Awal

Faculty of Mechanical Engineering, Universiti Teknologi Malaysia, 81310 Skudai, Johor Bahru, Malaysia

Received: 24 Oct. 2017, Revised: 25 Nov. 2017, Accepted: 20 Dec. 2017

ABSTRACT: Unmanned rotary-wing aircrafts or rotorcrafts are often prone to diverse atmospheric turbulences, and undeniably, abrupt gusts are reckoned to be the most acquainted commotion of them. Time and again, gust turbulence have dictated being the regulating trigger for countless mishaps concerning micro aerial vehicles. Given that the core/main rotor provides principal lift along with governing directional control and dynamic stability for any rotorcraft, the demeanors of thrust or induced air-flow through the gyrating blades largely signify the barebones of its functionality. This paper presents an idiosyncratic approach towards reviewing the impact of wind gust on rotor induced aerodynamic flow performance of an unmanned rotorcraft. Artificial gusts have been generated through the inherent concept of forced pitched oscillation without the use of any conventional wind tunnel. Gust air-speed and the rotor induced air-speed are gauged through the same contraption to provide homogeneous quantitative valuation. Each rotor-halves have been assessed 'root-to-tip' across designated span-wise positions against selected strengths of gust. Comparative analysis with normal atmospheric condition indicated gradual loss of cumulative thrust during hover (15-40%) and forward flight (10-30%) within the stipulated gust range and infers the risk of declining altitude. Protuberant imbalance of thrust across the rotor disk during hover indicated the likelihood of lackadaisical half-pitched rolling motion. However, during forward flight, the reduced discrepancy of thrust between the rotor halves signified gradual loss of cruising speed with regards to the increasing gust strength for the specific rotorcraft model. Experimental findings in this study exhibited prospect of appraisal with full-scale rotorcrafts.

Keywords: Rotorcraft, Gust wind, Induced flow, Rotor blade, Air speed

1. INTRODUCTION

The aerodynamics concurrent with rotorcrafts or helicopters happens to be rather befuddling and it is presaged that the engendered rotor wakes may conceivably be stronger than those formed by a fixed-wing aircraft of the same weight [1], [2]. Perilous catastrophes concerning rotorcrafts have become more of a recurring matter as a consequence of mechanical, electrical or structural failure. Besides, every so often environmental disturbances play a domineering role in rotorcraft related accidents where gust hindrance transpires to be one of the foremost natural cause. According to Voogt and Doorn [3], full scale helicopter accidents are predominantly dependent on different types of operation; where a majority of fatal incidents during flight are associated to the weather. Mashman [4] on the other hand, stated that the most common forms of turbulence faced by pilots include strong surface winds and gradient winds, where downdrafts and microbursts present a bigger threat to helicopters compared to fixed-wing aircrafts. Unmanned/micro rotary-wing aerial vehicles on the other hand, are much more vulnerable to aggressive environment than a full scale helicopter in flight.

Most of the contemporary reports involving rotorcrafts in challenging environment are typically leaned towards autonomous control and disturbance rejection requirements [5]-[10]. However, literature concerning rotorcrafts against simulated wind gusts is rather curbed, especially when it comes to analyzing the rotor induced air-flow [11]-[13]. This is primarily owing to the fact that conducting aerodynamic tests on rotorcrafts, particularly in wind tunnels, often proves to be intricate and pricey.

1.1 Gust Wind

Wind is, by and large, an idiosyncratic and tangible circulation of air wafting from a particular trajectory [14]-[16]. Gust wind on the other hand, is considered to be an abrupt and ephemeral upsurge in wind velocity within a specified period of time [17]-[19]. To characterize gusts in general, the peak wind speed is required to reach at least 16 knots (8.23 ms^{-1}) where the variance between the peak and lull wind speed needs to be a minimum of 9 knots (4.63 ms^{-1}), while maintaining a duration no greater than 20 seconds [20]-[22].

1.2 Simulated Artificial Wind Gust

Research on gust generation have received attention from various engineering standpoints. Numerous wind tunnels have been designed and

built throughout the years, including multi-purpose, low-speed and open-loop wind tunnels capable of measuring turbulence, flow rate and pressure in the test section in order to study an assortment of engineering objects [23]-[25]. Pertinently, when it comes to artificial gust generation, research work conducted by Neumann and Mai [26] stands out from the rest. In this study, the researchers performed experiments through the utilization of a transonic wind tunnel at Gottingen-Germany, capable of generating flow speeds from 0.3 Ma to 1.8 Ma. The key constituent of this wind tunnel is a built-in airfoil that can be excited in order to force the air with a resulting wake, which however is the generic gust. This oscillating airfoil is equipped to execute different aerodynamic excitations which can be harmonic or transient in nature. The airfoil, having a cross-sectional form of NACA0010, was mounted upstream of the wind tunnel in order to operate as a gust generator. Here, the hydraulic exciters operates in phase opposition, which abets in varying the symmetrical airfoil's angle of attack. When it comes to forced pitched oscillation, this gust generator has a maximum frequency (*f*) of 60 Hz. Even though this experimentation involved reviewing the effects of synthetic gust on a wing model; the method utilized here to generate generic wind gusts can be considered one of most apposite ways to conduct this kind of investigation involving any relevant entities as 'test-specimen'. Fig.1 demonstrates the schematic representation of Neumann and Mai's gust experiment set-up.

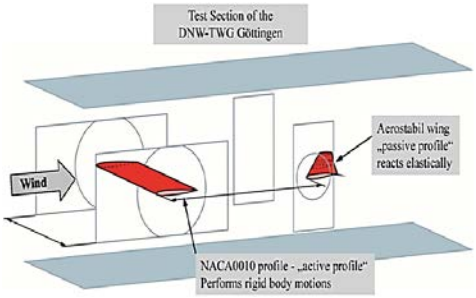

Fig.1 Schematic of Neumann and Mai's synthetic gust experiment set-up on a wing model [31]

1.3 Research Significance

The usage of rotorcrafts have skyrocketed in the recent past not only in military applications but in our daily lives as well [27], [28]. Rotary-wing unmanned aerial vehicles (RUAVs) are rapidly finding their way to provide assistance in every possible spectrum imaginable including aerial imagery & mapping, surveillance, infrared thermography in construction industry, product shipping/delivery and many more [29]-[32]. With the increased usage, comes the price of escalated number of mishaps as well; where natural or environmental disturbances, especially whether related turbulences, tops the list of reasons [3], [33]. Despite the fact that rotor aerodynamics plays an important role in understanding the rotorcraft's behavior with respect to the air flow, available research work on the related theme is rather limited and implores for attention. In view of that, this paper aims to provide an insight into the rotor air flow characteristics across the blade span in response to artificially generated wind gusts. This is to gain a developed understanding of the matter in question, which could possibly be referred not only amongst drones or RUAV's, but with full scale operational helicopters in some measure as well.

2. METHODOLOGY

The concept of forced pitched oscillation suggests that, an oscillating airfoil or wing is able to generate gust wave while being subjected to continuous flow of air [26]. This principle happens to be one of the most fundamental approach towards generating artificial wind gusts. Ordinarily, gust generated through manual or artificial mechanism is characterized through the features of frequency, amplitude etc. Here, the referring speed is mostly limited to the 'source' air-speed. However, it's a cogent inference that the air-speed would somewhat vary from prior to post encounter of the oscillating airfoil/wing. Meaning that, the wake of the airfoil would have a different air-speed than that from the source. Neumann and Mai [26], implemented particle image velocimetry (PIV) technique to measure the change in flow velocity by studying the flow field behind the gust generator. However, the investigation seemed to be deficient in both idiosyncratic and concurrent valuation which could be associated with the aerodynamic performance of the test specimen in an analogous manner.

Predominantly attributable to the matter of accessibility, pragmatism, cost and ancillary limitations; this paper presents an unambiguous experimentation approach which has been conceived devoid the use of an actual wind tunnel to generate artificial gust and quantify the rotor induced air velocity.

2.1 Test Set-up

Fig.2 illustrates the summarized schematic diagram for the set-up conceived for the experiment. In this set-up, the steady flow of air is provided by an 850 W industrial blower (fundamental features are listed in Table 1). Positioned in front of the blower is a symmetrical airfoil. Noticeably, the leading edge of the airfoil is facing directly towards the outlet of the air blower. Here, when the blower diffuses perpetual flow of air, the airfoil's wake is capable of producing gust wave of different

strengths while being oscillated at various frequencies. The airfoil is in fact oscillated using an astute combination of motor and linkage arm. The number of oscillation (or the frequency) of the airfoil is stalwartly related to the rotation/speed of the 100 W motor; which however, is regulated using a 13 khz speed controller. Here, instead of calling the oscillating airfoil a wing or vane, it is denoted as the 'Gust Generating Airfoil' or simply GGA. Crafted from thin aluminum sheet, this GGA is in fact shaped in the form of a NACA0014 airfoil section. The primary reason behind selecting a symmetrical airfoil is to generate a rather homogeneous wave of gust, while minimizing the variance between the magnitude of positive and negative peaks. Besides, generating gust through this mechanism has a likelihood of producing sinusoidal gust waves [26]. The GGA has a span of 0.45 m with a chord length of 0.1 m. Prior to oscillation, the pitching axis of the GGA is set to be located at the ½ chord length. Some elemental analysis have been performed on the GGA in order to identify certain parameters including maximum lift coefficient (Cl_{max}), maximum angle of attack (α_{max}) etc. Technical features of the GGA are summarized in Table 2. Congruently, specification of the motor and the speed controller designated for oscillating the GGA are enlisted in Table 3 and Table 4 respectively. It is understood that, the distance between the blower and the GGA will have a certain amount of effect on the strength of the gust. What's more, the distance from the GGA's trailing edge would have a distinct impact on the gust air-speed as well. This suggests that the strength of the wake or in this case the gust strength endured by the test object would actually vary with the increasing or decreasing gap between the GGA. Appositely, the test object in this case is an unmanned twisted blade co-axial (2+2) helicopter capable of producing a maximum gyration speed of ± 2500 RPM expending a 7.4 V 1500 mAh battery as power source. Table 5 summarizes the specifications of the test helicopter. Now, ahead of placing the subscale helicopter downstream of the GGA; the strength or the flow velocity of the blower and the gust air-speed generated by the oscillating GGA requires to be quantified at alterable gap(s) between each other. Pertinently, for this research, an anemometer (Model: Skywatch Xplorer 2, accuracy ± 3%) is used to measure all germane air-speed/velocity.

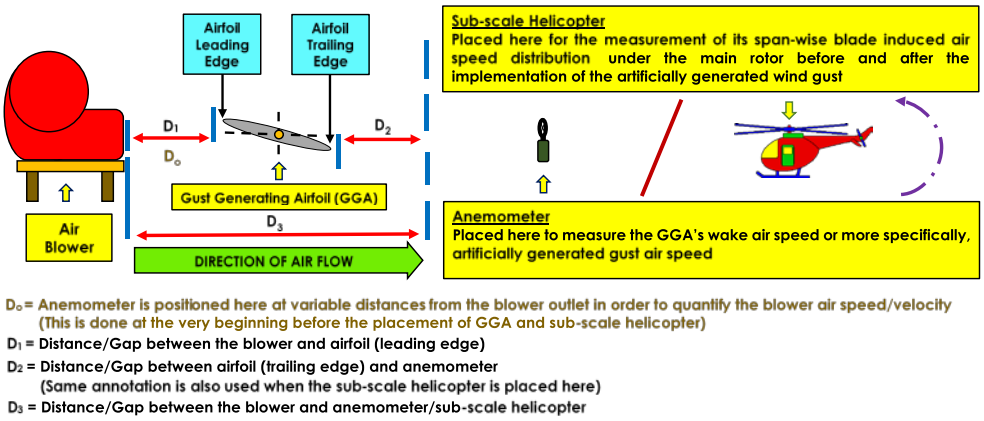

Fig.2 Comprehensive schematic representation of the gust experiment set-up and procedure

Table 1 Technical parameters of the air blower

Item	Specification
Model	Ogawa (BF534).
Voltage	220V-240V 50/60Hz
Current	4A
Power	850W
RPM	L – 1080; M – 1200; H - 1350

Table 2 Fundamental features of the GGA

Item	Specification
Airfoil Cross-section	NACA0014
Span	0.45 m
Chord Length	0.10 m
Pitching axis location	At ½ chord length
Maximum lift coefficient (Cl_{max})	(≈) 1
Maximum angle of attack (α_{max})	± 13°

Table 3 Specification of the motor designated for oscillating the GGA

Item	Specification
Motor Type	Brush Non-gear Hub
Voltage	24 V
Rated Power	100 W
No load current	< 0.55 A
No load speed	3500 rpm
Rate torque	0.35 N.m
Rate speed	2800 rpm
Rate current	< 6.0 A
Efficiency	> 68 %
Transmission	Chain Sprocket (9 teeth, pitch 6.35 mm)

Table 4 Specification of the motor speed controller

Item	Specification
Voltage Input	12 V - 40 V
Power	400 w
Current	8 A (Rated) , 10 A (Max)
Frequency	13 khz
PWM Duty Cycle	10-100%

Table 5 Specifications of the test helicopter

Item	Specification
Rotor Formation	Coaxial
Rotor Radius	0.26 m
Chord Length	0.044 m
Blade Type	Twisted
Overall Length	0.75 m
Overall Height	0.30 m
Fuselage Length	0.30 m
Number of Blades	2 + 2
Primary Control	Lower Rotor
Power Source	7.4 V 1500 mAh Li-poly
RPM (Max)	±2500

2.2 Quantitative Data Gauging Procedure

The induced air flow underneath the main rotor is, in actual fact, the thrust that assertively provides lift for the helicopter. During gust loading, understandably, this thrust would be affected to certain extent. Signifying that the main rotor blade induced air flow needs to be evaluated both before and after the implementation of artificially generated wind gust. Here, the blower air-speed is the first set of data that is required to be collected. Refereeing back to Fig.2, prior to the inclusion of the GGA and subscale helicopter in the arrangement of the test set-up, the anemometer is positioned in front of the blower. The air-speed is then measured at variable distances (D_o) from the outlet for three basic regulated speed range; this includes - low (1080 rpm), medium (1200 rpm) and high (1350 rpm). Soon after determining the blower range and capacity, the GGA is then positioned in front of the blower. D_1, D_2 and D_3 in this case correspondingly refers to: the gap between the blower & airfoil's leading edge; the gap between airfoil's trailing edge & anemometer; and the gap between the blower & anemometer. These gaps are varied while the GGA is oscillated at a range of harmonic excitations in order to regulate and quantify the different strengths of gust that is being generated.

As the minimum required air-speed for gust is 8.23 ms^{-1} (or 16 knots) [20]-[22], three strengths of gust have been deliberately decided on for this investigation, these are: 8.5 ms^{-1}, 9.0 ms^{-1} and 9.5 ms^{-1} respectively. Using a fitting gap between D_1 and D_2, a data-cluster is created with an array of GGA oscillation frequencies along with their corresponding air-speed. This data abets in determining the required frequencies for the specified strengths of gust through interpolation or extrapolation. Once the concomitant oscillation frequencies are determined, only then, the rotorcraft is placed downstream of the GGA for quantitative assessment. Appositely, the maximum angle of attack for the GGA has been limited to $\pm 10^o$ using the linkage arm connected to the motor; so if the leading edge start from $+10^o$, then pitched down to -10^o and then again pitched back up to $+10^o$ it would have completed one oscillation. Refereeing to Fig.3, the simulated gust strength is measured downstream of the GGA at the horizontal level for both 'pitched up' and 'pitched down' airfoil positions. These level positions are demarcated as 'positive phase' (GGA trailing edge pitched up & leading edge pitched down) and 'negative phase' (GGA trailing edge pitched down & leading edge pitched up).

Based on the effectiveness, a rotor blade can be divided into three sections. Moving from the center to the outer tip of the main rotor, 25% of the blade span is stall region, 45% of the blade span is the driving region and 30% of the blade span is driven region [1]. As the lower rotor provides primary control for the test helicopter, therefore the half-rotor blade is also divided into comparable segments. Fig. 4 shows the schematic illustration of the measurement points for the half-rotor blade. Starting from the root, the three regions are divided into a total of eight measurement points. The stall region hosts the first two points: point 1($P_{1[stall]}$) and point 2 ($P_{2[stall]}$). Subsequently, the driving and the driven regions are divided into three points each. Here, points 3, 4, 5 (or $P_{3[Drive]}$, $P_{4[Drive]}$, $P_{5[Drive]}$ respectively) are located in the driving region; followed by points 6, 7, 8 (or $P_{6[Driven]}$, $P_{7[Driven]}$, $P_{8[Driven]}$ respectively) which are located in the driven region. For static gauging, the remote controlled rotorcraft is fixed on a test rig at a dedicated testing space. Flight conditions for the rotorcraft is achieved through its designated wireless controls. When the lift distribution is in

question, the rotor disk is apportioned into 'right-hand & left-hand' side (or R-H-S & L-H-S) followed by 'forward/advancing & aft/retreating' side (or F/A-S & A/R-S) when viewed from front and sideways respectively. Appositely, in each context, gusts are set to be introduced horizontally from the R-H-S flowing towards the main rotor. During hover, the lift is commonly expected to be balanced in each sides. However, during turning flight, lift force is side-biased depending on the maneuvering direction. Understandably so, if lift distribution was homogenous, there wouldn't be any trajectory force vectors and thus no directional motion of any kind. Fig.5 depicts the segmentation of helicopter rotor during flight from basic directional point of view.

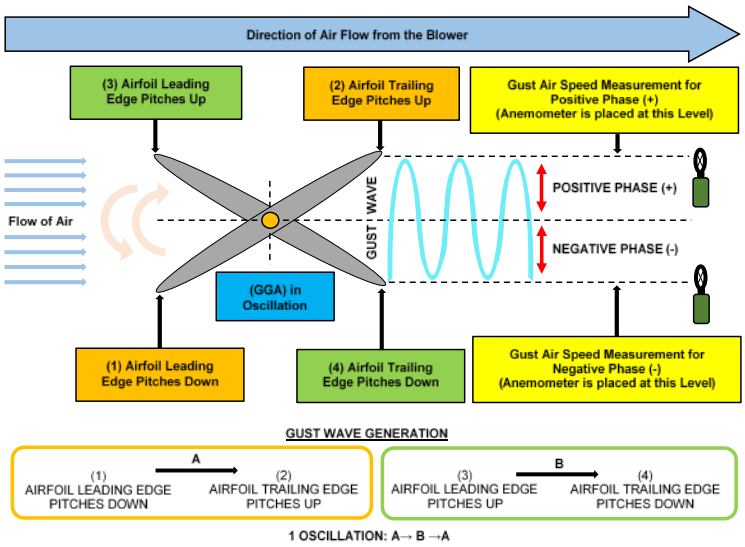

Fig.3 Oscillation mechanism for the GGA and the phase position(s) for gauging gust air-speed

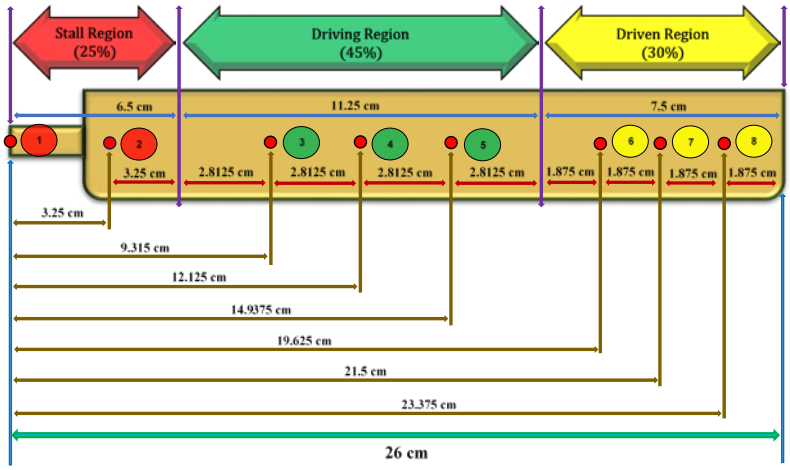

Fig.4 Schematic representation of 'Root → Tip' measurement points for half rotor blade

(a) Front View (b) Side View

Fig.5. Segmentation of helicopter rotor during flight: (a) R-H-S & L-H-S (b) F/A-S & A/R-S

3. RESULTS AND DISCUSSION

3.1 Artificially Generated Wind Gust

The relationships between the blower air-speed and the distance from its outlet - [D_o] at differential motor speeds are shown in Fig 6. Here, within a meter range, the air velocity subsides gradually while moving away from the outlet. The highest velocity (18.1 $ms^{-1)}$ occurs at close vicinity when the motor speed is set at 'high (or 1350 rpm). This eventually ascertains the fact that the blower is adept of producing the required strength(s) of gust for the principal experimentation.

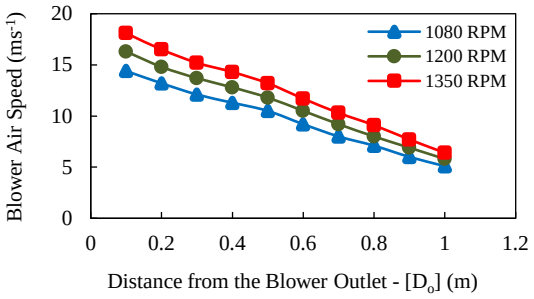

Fig.6 Blower air-speed versus varying distance from the outlet for a range of motor speeds

The 3D schematic manifestation of the test arrangement to measure the simulated gust loads is shown in Fig.7. Gust air-speed is quantified with regards to the positive and negative phase for each gap. The values for the negative phase are assigned negative magnitudes in order to provide a coherent distinction from the positive phase quantities. The gust air-speed against varying distance between the GGA and anemometer - [D_2], with respect to the sequential shifting of the gaps in-between the blower and the GGA - [D_1] is plotted in Fig.8. The data for positive and negative phase are coalesced together with regards to their corresponding positions. The GGA is arbitrarily oscillated at 1.5 Hz (in this case, 45 oscillations per 30 seconds) for each measurement. From Fig.8, it can be noticed that the gust air-speed wanes gradually while moving away from the GGA (i.e. increase in D_2). This reduction in the gust air-speed appears to be much more perceptible when the gap between the blower and the GGA is altered (i.e. increase in D_1). There are perceptible variations in the positive and negative phase values which are conceivably owing to the common manufacturing erroneousness; these variations are still exceedingly peripheral and negligible to some extent.

Next, the gust air-speed is measured again, but this time with reference to GGA frequency (*f*) of 0.5 Hz, 1.0 Hz, and 1.5 Hz for both positive and negative phase respectively. This abets in forming a data-cluster which enables to identify the frequencies corresponding to the stipulated gust strengths though interpolation or extrapolation within the maximum pitching restraint of ±10°. For each frequency, the ceiling for delineated time-span is 30 seconds. A reading is taken every 5 seconds for each phase until the cycles are completed separately. Constant gap for D_1 (0.1 m), D_2 (0.1 m) and D_3 (0.3 m) are perpetually maintained in order to circumvent gradual attenuation of gust strength.

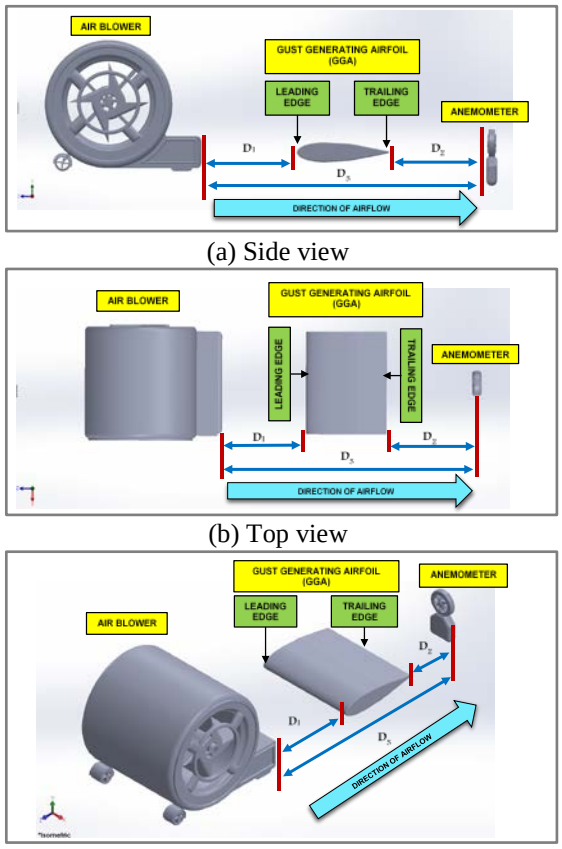

(a) Side view

(b) Top view

(c) Isometric view

Fig.7 Schematic manifestation of the test arrangement to quantify artificially generated gust

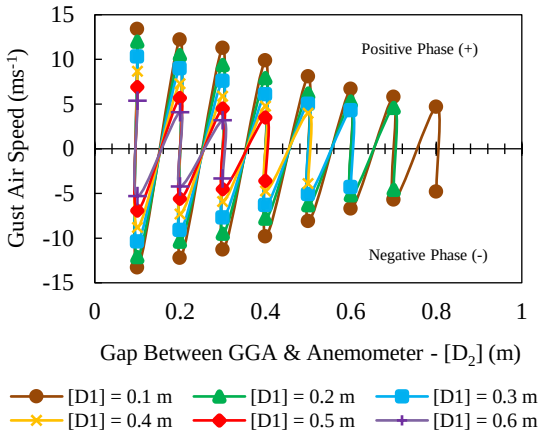

Fig.8 Combined positive-negative phase of gust air-speed against varying gaps of [D_2] and [D_1]

The gust air-speed against time for 0.5 Hz, 1.0 Hz and 1.5 Hz of GGA frequency (f) is given in Fig.9. Here, the highest and lowest strengths of gust transpire against the highest and lowest frequencies respectively. The required frequencies are then calculated using the data-cluster. By means of interpolation, 8.5 ms^{-1}, 9.0 ms^{-1} and 9.5 ms^{-1} of gust requires a GGA frequency of (≈) 1.0 Hz, (≈) 1.2 Hz and (≈) 1.3 Hz respectively. The fractions are avoided to form even values. These values however, correspond to the peak values set to be exhorted on the subscale helicopter. As the variance between peak and lull requires to be greater than 4.63 ms^{-1} [20]-[22], therefore, a common lull (3.9 ms^{-1}) is designated against all the other peak values. Generated at (≈) 0.5 Hz, this air-speed of 3.9 ms^{-1} provides a difference greater than 9 knots (or > 4.63 ms^{-1}) between the peak(s) and lull(s). During the simulation of wind gust on the test helicopter, each peak and lull values are manually given a period of 5 seconds to complete a singular cycle of 10 seconds. While forming a square waveform signal of transient state through concurrent assimilation of peak and lull values. The specified ranges of simulated wind gusts against coordinated time span accounted for the experimentation are described in Fig.10.

3.2 Rotor Induced Aerodynamic Flow

The thrust or induced aerodynamic flow through the rotor eventually provides lift by staying true to Newton's Third Law of Motion. Therefore, gauging the span-wise air-speed/velocity underneath the rotor essentially presents an overview of the lift distribution. The graphic representation of the test set-up for quantitative investigation concerning the effects of simulated wind gusts on the rotor induced air flow performance of the test helicopter during hover and forward flight is included in Fig.11.

3.2.1 Hovering Flight State

In Fig.12, the span-wise induced air-speed(s) are plotted against their demarcated position(s) during hover. In normal condition, $P_{2[stall]}$ through $P_{6[Driven]}$ indicated steady rise in rotor induced velocity, followed by its gradual attenuation through $P_{7[Driven]}$ and $P_{8[Driven]}$ for both R-H-S and L-H-S. Positions $P_{4[Drive]}$, $P_{5[Drive]}$ and $P_{6[Driven]}$ recorded the highest magnitudes in the driving and driven region without any surrounding gusts. When gusts are introduced, $P_{8[Driven]}$ on the R-H-S remains closest to the release zone. Here, for each gust loading, $P_{8[Driven]}$ reveals no presence of thrust/lift. $P_{1[stall]}$ and $P_{2[stall]}$ indicated rebuffed input in lift generation. Perpetual increase in gust strength points out loss of cumulative thrust on the R-H-S. Cumulative thrust is essentially the area under the curve from $P_{1[Stall]}$ through $P_{8[Driven]}$.

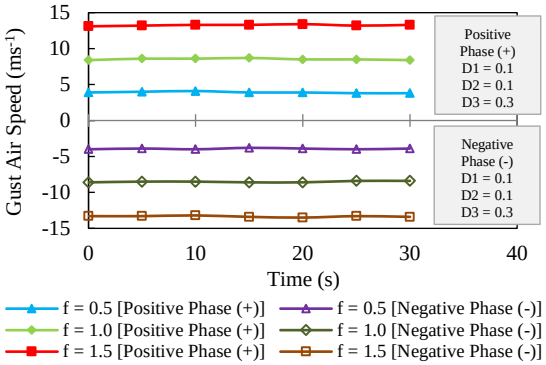

Fig.9 Gust air speed versus time with regards to an array of oscillation frequencies

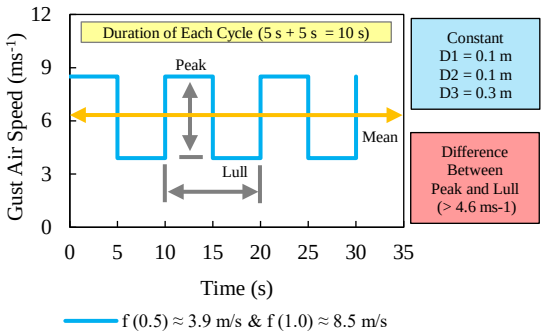

(a) Contrived gust wave with 8.5 ms^{-1} peak (f ≈ 1.0 Hz) and 3.9 ms^{-1} lull (f ≈ 0.5 Hz)

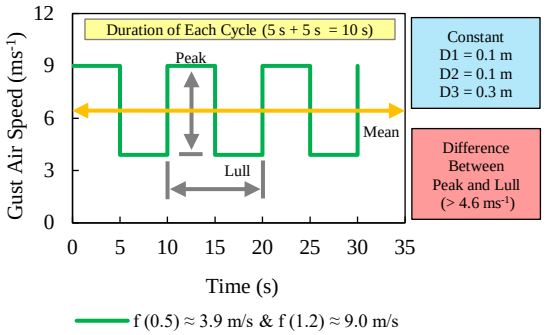

(b) Contrived gust wave with 9.0 ms^{-1} peak (f ≈ 1.2 Hz) and 3.9 ms^{-1} lull (f ≈ 0.5 Hz)

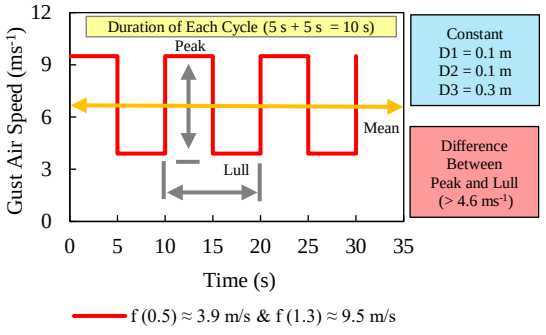

(c) Contrived gust wave with 9.5 ms^{-1} peak (f ≈ 1.3 Hz) and 3.9 ms^{-1} lull (f ≈ 0.5 Hz)

Fig.10 Gust air-speed against synchronized time span simulated through harmonic oscillation

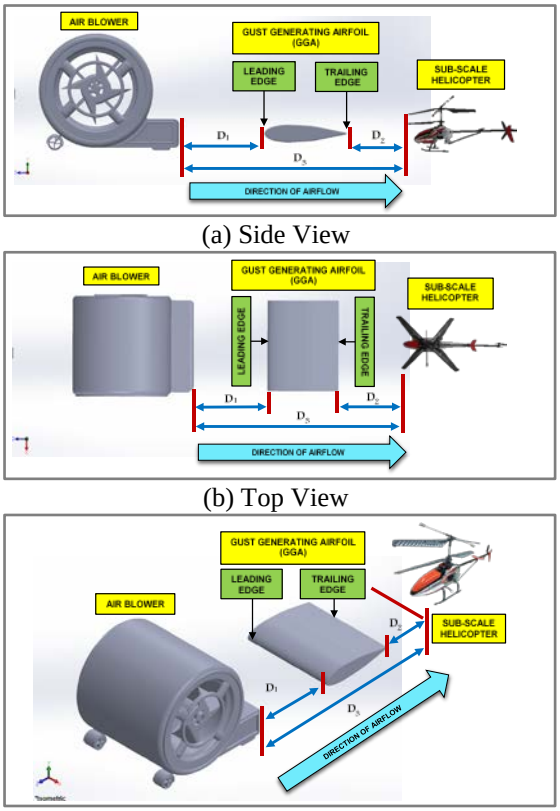

(a) Side View

(b) Top View

(c) Isometric View

Fig.11 Schematic interpretation of the gust-test arrangement intended for the designated helicopter

The effect of gust is not as flashy on L-H-S as compared to R-H-S. When gusts are introduced, L-H-S loses approximately 15% to 30% of cumulative thrust compared to normal condition; whereas, R-H-S loses around 40 % to 70 % of total thrust. Loss of thrust signifies loss of altitude. Evidently, R-H-S loses around 15 % to 40 % more thrust compared to L-H-S. This imbalance of thrust/lift will cause the helicopter to experience half-pitched rolling susceptibility during gust loading. To avert any rollover, the gust endured side must gain or the opposite side must lose lift rapidly. Conceivably, this can be achieved by using rotor blades with morphing capabilities where this original idea utterly begs for introspective research.

3.2.2 Forward Flight State

The blade induced air flow is quantified from $P_{1[Stall]}$ until $P_{8[Driven]}$ during forward flight and plotted through the graph(s) in Fig.13. In normal condition, the thrust/lift distribution indicates similar pattern from 'root-to-tip' compared to hover, where there is a steady rise past the stall region and followed by gradual waning beyond the half rotor blade span. There is, however, imbalance of total thrust between the sides, where F/A-S generates almost 20 % less thrust compared to A/R-S.

Nevertheless, this disparity between the sides is essential in achieving forward motion as the force vector components are resolved with regards to the tilted rotor. In fact, the resolution of vector forces is a typical requirement for a rotorcraft in order to achieve any kind of directional flight.

During gust loading, $P_{1[Stall]}$ and $P_{2[Stall]}$, remains inept in lift generation. On the driving region, $P_{3[Drive]}$ emerges to lose lift for each sides during 9.5 ms^{-1} of gust . This implies that, for increasing gust, the gradual attenuation of thrust/lift may occur from root-to-tip of the rotor blade. With regards to the rising gust strength, F/A-S loses around 20 % to 50% of thrust; whereas for A/R-S, this loss is around 10 % to 30%. This indicates that there will be significant reduction in altitude during gust loading. These loads also cause the reduction in the variance (less than 20 %) of thrust between F/A-S and A/R-S signifying the decline of magnitude for directional force vector component. Hence, the rotorcraft will also tend to lose cruising speed in response to the increasing gust loads.

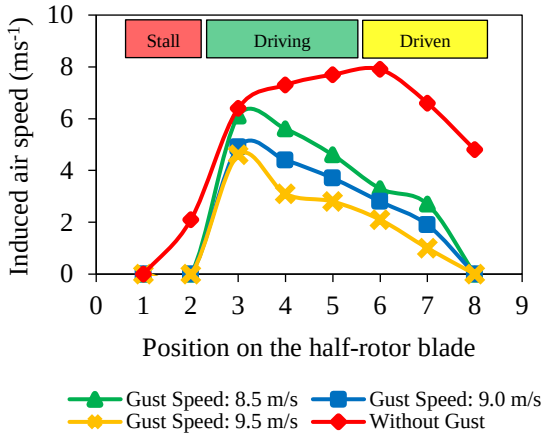

(a) R-H-S

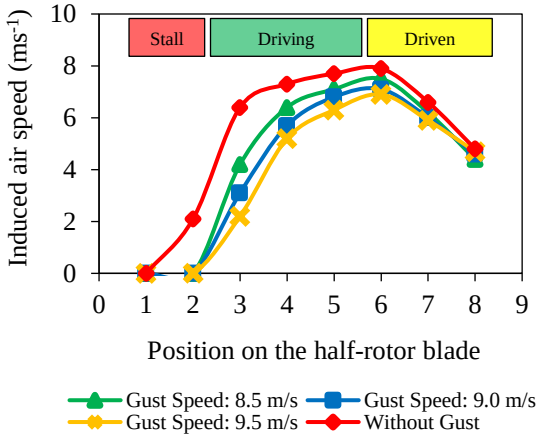

(b) L-H-S

Fig.12 Blade induced air-speed against marked span-wise positions with regards to differential gust loading during hover

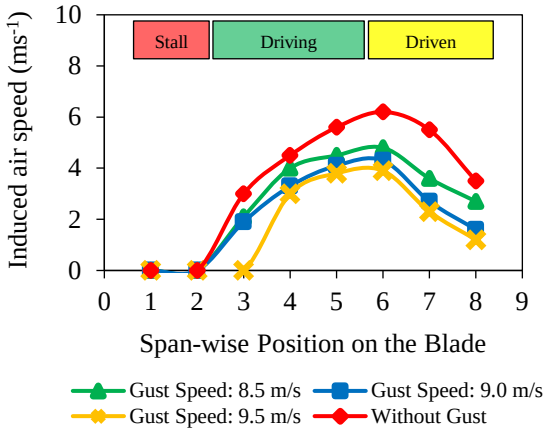

(a) F/A-S

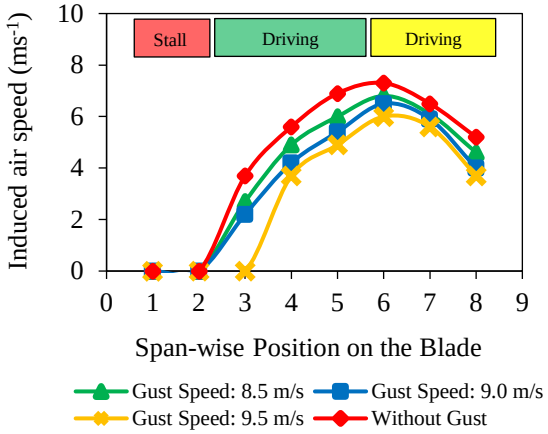

(b) A/R-S

Fig.13 Blade induced air-speed against marked span-wise positions with regards to differential gust loading during forward flight

4. CONCLUSION

In this study, artificial gusts were generated through forced pitched oscillation in order to review its effects on an unmanned helicopter's rotor induced flow performance. Within the specified gust range, the following conclusions could be drawn based on the findings:

i. During hovering state, the cumulative magnitude and distribution pattern of the induced air-speed/thrust/lift indicated the risk of declining altitude and half-pitched rolling motion within the gust duration for the specified rotorcraft.
ii. During forward flight state, for the same governing factors, the rotorcraft indicated liability to declining altitude, along with the reduction in cruising speed as well.

5. ACKNOWLEDGEMENTS

The author wishes to acknowledge the technical support received from Dr Mohd. Shariff bin Ammoo and Assoc Prof Dr Shuhaimi bin Mansor in conducting the research work.

6. REFERENCES

[1] Ammoo M.S.b. and Awal Z.B.A. Main Rotor Blade Air Flow Characteristics & Behaviour of a Remote Controlled Sub-Scale Helicopter: A Case Study, International Journal of Research in Aeronautical and Mechanical Engineering, Vol.1, No.7, 2013, pp.228-235.

[2] Awal Z.B.A. and Ammoo M.S.B., A Case Study on the Air Flow Characteristics of the Hirobo-FALCON 505 Controllable Helicopter's Main Rotor Blade, Applied Mechanics and Materials, Vol.527, Feb. Issue, 2014, pp.39-42.

[3] Voogt A.D. and Doorn, R.R.A.V., Helicopter accidents: Data-mining the NTSB database, in Proc. 33rd European Rotorcraft Forum, 2007, pp.1-7.

[4] Mashman J., Helicopters and turbulence, Flight Safety Foundation's Helicopter Safety, Vol.14, No.5, 1988, pp.1-2.

[5] Lusardi, J., Tischler M. and Blanken C., Empirically Derived Helicopter Response Model and Control System Requirements for Flight in Turbulence, Journal of American Helicopter Society, Vol.49, No.3, 2004, pp.340-349.

[6] Alexis K., Nikolakopoulos G., Koveos Y. and Tzes A., Switching Model Predictive Control for a Quadrotor Helicopter under Severe Environmental Flight Conditions, IFAC Proceedings Volumes, Vol.44, Jan. Issue, 2011, pp.11913-11918.

[7] Muñoz F., Hernández I.G., Salazar S., Espinoza E.S. and Lozano R., Second Order Sliding Mode Controllers for Altitude Control of a Quadrotor UAS: Real-Time Implementation in Outdoor Environments, Neurocomputing, Vol.233, Apr. Issue, 2017, pp.61-71.

[8] Faiçal B.S., Freitas H., Gomes P.H., Mano L.Y., Pessin G., Carvalho A., Krishnamachari B. and Ueyama J., An Adaptive Approach for UAV-based Pesticide Spraying in Dynamic Environments, Computers and Electronics in Agriculture, Vol.138, Jun. Issue, 2017, pp.210-223.

[9] Mokhtari M.R., Cherki B. and Braham A.C., Disturbance Observer based Hierarchical Control of Coaxial-Rotor UAV, ISA Transactions, Vol.67, Mar. Issue, 2017, pp.466-475.

[10] Shin Y.H., Lee S. and Seo J., Autonomous Safe Landing-Area Determination for Rotorcraft UAVs using Multiple IR-UWB Radars, Aerospace Science and Technology, Vol.69, Oct. Issue, 2017, pp.617-624.

[11] Tang D.M. and Dowell E.H., Nonlinear Response of a Non-Rotating Rotor Blade to a Periodic Gust, Journal of Fluids and Structures, Vol.10, No.7, 1996, pp.721-742.
[12] Yang X., Garratt M. and Pota H., Flight Validation of a Feedforward Gust-Attenuation Controller for an Autonomous Helicopter, Robotics and Autonomous Systems, Vol.59, No.12, 2011, pp.1070-1079.
[13] Zarovy S., Costello M. and Mehta A., Experimental Method for Studying Gust Effects on Micro Rotorcraft, Proceedings of the Institution of Mechanical Engineers, Part G: Journal of Aerospace Engineering, Vol.227, No.4, 2012, pp.703-713.
[14] Zerrahn A., Wind Power and Externalities, Ecological Economics, Vol.141, Nov. Issue, 2017, pp.245-260.
[15] Ren G., Liu J., Wan J., Guo Y. and Yu D., Overview of Wind Power Intermittency: Impacts, Measurements, and Mitigation Solutions, Applied Energy, Vol.204, Oct. Issue, 2017, pp.47-65.
[16] Hagen N., Passive Imaging of Wind Surface Flow using an Infrared Camera, Infrared Physics & Technology, Vol.87, Dec. Issue, 2017, pp.47-54.
[17] Emejeamara F.C., Tomlin A.S. and Hopkins J.T.M., Urban Wind: Characterisation of Useful Gust and Energy Capture, Renewable Energy, Vol.81, Sept. Issue, 2015, pp.162-172.
[18] Bardal L.M., Sætran L.R., Wind Gust Factors in a Coastal Wind Climate, Energy Procedia, Vol.94, Sept. Issue, 2016, pp.417-424.
[19] Pagnini L.C., Piccardo G., A Generalized Gust Factor Technique for Evaluating the Wind-Induced Response of Aeroelastic Structures Sensitive to Vortex-Induced Vibrations, Journal of Fluids and Structures, Vol.70, Apr. Issue, 2017, pp.181-200.
[20] Mark L., The Book of Hierarchies, 2nd ed., William Morrow and Co. Inc., 1984, pp.92.
[21] Morris C.G., Dictionary of Science and Technology, 1st ed., Academic Press Inc., 1992.
[22] Bomar G.W., Weather in Texas: The Essential Handbook, University of Texas Press, 1st ed., 2017.
[23] Kobayashi H. and Hatanaka A., Active Generation of Wind Gust in a Two-Dimensional Wind Tunnel, Journal of Wind Engineering and Industrial Aerodynamics, Vol.42, Oct. Issue, 1992, pp.959-970.
[24] Inan A. T., Design of Multi-Purpose Low Speed Subsonic Air Tunnel and Turbulence Measurements, Ph.D. Thesis, 2003, Marmara University, Istanbul.
[25] Bi Y., Xie C., An C. and Yang C., Gust Load Alleviation Wind Tunnel Tests of a Large-Aspect-Ratio Flexible Wing with Piezoelectric Control, Chinese Journal of Aeronautics, Vol. 30, Feb. Issue, 2017, pp.292-309.
[26] Neumann J. and Mai H., Gust Response: Simulation of an Aeroelastic Experiment by a Fluid-Structure Interaction Method, Journal of Fluids and Structures, Vol.38, Apr. Issue, 2013, pp.290-302.
[27] Hassanalian M. and Abdelkefi A., Classifications, Applications, and Design Challenges of Drones: A review, Progress in Aerospace Sciences, Vol.91, May Issue, 2017, pp.99-131.
[28] Vacca A. and Onishi H., Drones: Military Weapons, Surveillance or Mapping Tools for Environmental Monitoring? The Need for Legal Framework is Required, Transportation Research Procedia, Vol.25, May Issue, 2017, pp.51-62.
[29] Djaja K., Putera R., Rohman A.F., Sondang I., Nanditho G. and Suyanti E., The Integration of Geography Information System (GIS) and Global Navigation Satelite System-Real Time Kinematic (GNSS-RTK) for Land use Monitoring, International Journal of GEOMATE, Vol.13, No.36, 2017, pp.31-34.
[30] Bucknell A. and Bassindale T., An Investigation into the Effect of Surveillance Drones on Textile Evidence at Crime Scenes, Science & Justice, Vol.57, No.5, 2017, pp.373-375.
[31] Entrop A.G. and Vasenev A., Infrared Drones in the Construction Industry: Designing a Protocol for Building Thermography Procedures, Energy Procedia, Vol.132, Oct. Issue, 2017, pp.63-68.
[32] Tavana M., Damghani K.K., Arteaga F.J.S. and Zandi M.H., Drone Shipping versus Truck Delivery in a Cross-Docking System with Multiple Fleets and Products, Expert Systems with Applications, Vol.72, Apr. Issue, 2017, pp.93-107.
[33] Voogt A., Fatalities in General Aviation: From Balloons to Helicopters, 1st ed. Vol.6, Turk, Ed. Forensic Pathology Reviews, Humana Press, 2011, pp.169-179.